Available online at www.sciencedirect.com
SCIENCE DIRECT®
Journal of Computational Physics 191 (2003) 265–281
JOURNAL OF COMPUTATIONAL PHYSICS
www.elsevier.com/locate/jcp

Application of Gaussian quadratures to density functional (df) theories of confined liquid crystals

Agnieszka Chrzanowska

Institute of Physics, Kraków University of Technology, ul. Podchorążych 1, 30-084 Kraków, Poland

Received 3 September 2002; received in revised form 21 March 2003; accepted 3 June 2003

Abstract

We present a technique to conduct the density functional analysis of a liquid crystal system under the constraints of two parallel walls. The key feature of our approach is the way to perform multidimensional integrals in which certain regimes of the arguments are forbidden due to the effect of the wall excluded volume. This effect occurs in the surface potentials that contain orientationally dependent hard cores. The proposed calculations are based on the exact Gaussian quadratures and application of the modified limits of integration. They are quick and efficient and give reasonable orientation-density distribution functions for a relatively small number of the integration grid points. Another benefit of the proposed method is the fact that neither polynomial expansions nor interpolations of the integral elements is needed and the resulting solution for the distribution functions is only endowed by the error of the second virial approximation. Application of this algorithm can be extended to soft interactions by using the hard core cutoff of the soft potentials as the limits of integration.
© 2003 Elsevier B.V. All rights reserved.

PACS: 02.70.−c; 61.30.Pq

1. Introduction

If a molecular system is limited by a substrate the translational symmetry of the particles' density distribution is broken: the particles cannot go beyond the introduced wall. Their extreme positions at this side are dictated by the distance of the closest approach that comes from the assumed wall–particle interaction. With the increasing pressure of the fluid the nearest to the wall molecules tend to form a two-dimensional layer, which manifests itself as a peak in the density distribution plotted versus the direction perpendicular to the substrate. With a further increase of the pressure this layer can attain a liquid-like structure [1–5]. New subsequent layers can be also formed and, finally, a solid state is obtained [6]. Properties of such layers in dependence on the thermodynamical parameters like the pressure, the temperature or the density are known as adsorption phenomena [1–6]. If two confining walls come into question growth of the wetting

E-mail address: achrzano@usk.pk.edu.pl (A. Chrzanowska).

0021-9991/$ - see front matter © 2003 Elsevier B.V. All rights reserved.
doi:10.1016/S0021-9991(03)00316-4

layers can be proceeded by the spinodal phase transition that is associated to spontaneous condensation and formation of a liquid-like state of condensed fluid. The thermodynamical parameters at which such transition occurs are usually shifted in reference to the corresponding parameters that characterise a similar transition of the bulk fluid. The whole phenomena bears the name of the capillary effect [5–7]. Occurrence of the above aspects of confinement, the capillary effect and the pure adsorption, depends on the size of the pores in which the substance is immersed.

An interest in confined fluids based on the spherical interactions has been extended into the case, where interactions are anisotropic. The main motivation of such extension was the fact that hardly any physical system exhibits truly spherical molecular symmetry. Even nitrogen, which is commonly regarded as a perfect example of the spherically symmetric interactions, when confined in a graphite slit, it can undergo in an adsorbed monolayer the incommensurate–commensurate structural transition, which cannot be explained on the basis of only isotropic models [5].

Main features of the confined isotropic fluids as oscillating density profiles, growth of the wetting films or capillary condensation have been expected to find their counterparts in liquid crystals. One can also expect additional effects due to the long-range order that is present in liquid crystal phases. By means of computer simulations and the density functional (df) theory approaches they have already been discovered in nematogenic systems: a wall peak in the density distribution, the surface uniaxial–biaxial (UB) phase transition, the capillary nematisation and the growth of the wetting biaxial layer. The reports about these basic phenomena do not, however, encompass systematical studies on the adsorption isotherms at different particle–particle and particle–wall interactions, or on the multilayer structures which may occur at higher pressures. This requires much more work from the side of computer simulations as from the side of the df theory models.

The role and importance of the density functional approach in confined geometries can be best seen for the isotropic fluids. Large literature on this subject exists as well for the systems composed from the hard core interacting bodies as from the soft van der Walls particles [8]. It gives evidence that success of the df theory lies in their predictive power. For example, in 1977 the density functional theory of Ebner et al. [1,2] as the first predicted pre-wetting phenomena of the surface phase transition and the growth of thick films. Because these phenomena are strongly dependent on the thermodynamical parameters close to coexistence and because, probably, of an inaccurate knowledge of the coexistence curve of the bulk fluid in the early 80s, these conclusions were firstly denied as incorrect. Appropriate choice of the mentioned parameters allowed, however, to corroborate Ebner's predictions by the Monte Carlo simulations [4] and, later, by the non-local density functional theory [3] even up to the agreement of the density profiles. By now, the non-local df theory approach is a well-established tool to study the confined systems' properties [5].

The first works of non-phenomenological character on the confined liquid crystals, by Poniewierski and Holyst [9] and by Poniewierski [10], have also benefited from the density functional approach. They concern a fluid of hard rods in contact with a hard wall, in which the distribution functions are assumed uniaxial. Although the biaxiality has been neglected the Poniewierski df theory correctly predicts negative values of the uniaxial order parameter in the surficial area [11,12]. This fact was also the reason to check the possibility of the biaxial phase formation. Using bifurcation analysis Poniewierski [10] has showed that the uniaxial surface layer becomes unstable with respect to the formation of the biaxial phase at a bulk density 15% below the bulk isotropic–uniaxial nematic transition. Subsequent papers confirm that the biaxial surface order of hard elongated particles is a rule [12–16]. Simulating a system of hard rods by the Monte Carlo method Dijkstra and coworkers [14–16] have showed that in small slits the isotropic fluid undergoes a first order capillary nematisation transition which ends in a capillary critical point at the wall separations smaller than about twice the length of the spherocylinders. They observed only one density peak. Evidence on the multilayer formation in the hard Gaussian overlap (HGO) system of hard ellipsoids has been found both by the Monte Carlo simulations and the df theory in [12]. Using a special type of

scaling as proposed by Allen et al. [17], the authors of [12] have obtained the theoretical profiles of the order parameters in an astonishingly good agreement with the simulation results. What is more important, they showed in the df theory approach the possibility of the eigenvalue exchange phenomenon, which is responsible for the switch of the dominant symmetry axis. In the studied case of two identical walls this eigenvalue exchange takes place with respect to the number density. What is the main symmetry axis at low densities (the normal to the substrate Z axis), at higher densities becomes of the secondary meaning at the cost of the X axis, which now becomes principal. A similar to the above abrupt change of the symmetry axis, but at the same density, has been reported by Rodriguez-Ponce et al. [18] for a nematic in a pore under hybrid anchoring conditions. Here, however, the authors blame the Frank elastic energy of the director distortion for the resulting orientational profiles. Whereas it has been already acknowledged that variations of the order contribute to the elastic energy [19–21] (this effect has been omitted in discussion of the paper [18]), it is not clear at all whether the Frank director distortion energy can be used for the cases with discontinuous changes of the symmetry axis, once it has been established on the assumption of small changes of the continuously changing director [22]. In [16] Dijkstra et al. have also proposed a modification of the Monte Carlo simulation method for the particles in contact only with a *single* wall. This method allows to eliminate possible capillary effects and, as such, it is especially suitable for the studies of adsorption and wetting phenomena. The authors of [16] have applied their method to a system of hard spherocylinders of a length-to-diameter ratio of 15 and, as the firsts, showed the growth of the surface biaxial nematic in contact with the bulk isotropic phase. As they admit, however, their results are sufficient to give an answer neither on the complete wetting problem nor on the nature of the UB transition. An interesting outcome is that a simplified df theory Zwanzig model [14–16], in which the orientations of the particles are restricted only to three orthogonal directions, is capable to predict the key features of the capillary nematisation transition.

Different anchoring conditions attract special attention. Because of the technological relevance this field seems to be the mostly investigated on [23–36]. An illustrative example of the interplay of anchoring conditions, sample dimensions and microscopic organisation is given, for instance, in [34]. In this paper Gruhn et al. have presented snapshots of a nematic phase in the presence of the walls that favour homeotropic alignment. The authors show variations of the microscopic structure which depend on the wall separation distance and which are correlated with the normal component of the stress tensor.

Although the knowledge about confined nematics is quite substantial by now, much more work is necessary to learn about the effects arising from the particular interactions and anchoring conditions. The progress of theoretical studies on the coexistence, orientational wetting phenomena or phase transitions in the liquid crystals remaining in contact with a substrate depends mainly on the accuracy of the multidimensional integrations, which are inherent to the df theory self-consistency equations. The purpose of this work is to present the way to calculate these integrals in a manner as efficient as possible and, in the spirit of the Numerical Recipes [37], the *only* exact one.

The structure of the paper is as follows. In Section 2 we introduce basic concepts of the density functional theory. The polynomial expansion way of solving the self-consistency equations is given in Section 3. This section is given as a reference and review of the traditional method and addressed to the young researchers not acquainted with the details of the df theory. It presents also what difficulties can be expected in the case of inhomogeneous materials while using the traditional method. Extension of the Gaussian quadratures (GQ) idea for the case with adjusted angular limits is given in Section 4. Section 5 presents examples of the orientation and the density profiles obtained at different numbers of the grid points. How to apply the method to the df theories based on the Lennard–Jones type potentials (soft interactions with the orientation dependent steric cores) is shortly discussed in Section 6. Section 7 indicates a specifique case for which the performance of the Gaussian quadratures is lower than desired and, finally, in Section 8 we conclude by summarising the main idea and its possible applications.

2. Theory

We consider a system composed of anisotropic uniaxial particles confined between two structureless walls which are separated by the distance L. The state of each particle is described by its position $\mathbf{r}$ and its orientation vector $\mathbf{a}$. For the purpose of this work we will use as an example a simplified system in which the particles can interact only due to hard core interactions, as well among themselves as with the confining walls. This condition means that when a given particle overlaps with another particle or one of the walls, the interaction potential is assumed as infinite. Otherwise it is assumed as zero. This type of interaction leaves the shape of the molecules as the most important factor. In particular, the particle–particle interaction is characterised by the function of the closest approach of two bodies $\sigma(\mathbf{r}_{12}/|\mathbf{r}_{12}|, \mathbf{a}_1, \mathbf{a}_2)$

$$U_{12}(\mathbf{r}_{12}, \mathbf{a}_1, \mathbf{a}_2) = \begin{cases} 0 & \text{if } |\mathbf{r}_{12}| \geqslant \sigma(\frac{\mathbf{r}_{12}}{|\mathbf{r}_{12}|}, \mathbf{a}_1, \mathbf{a}_2), \\ \infty & \text{if } |\mathbf{r}_{12}| < \sigma(\frac{\mathbf{r}_{12}}{|\mathbf{r}_{12}|}, \mathbf{a}_1, \mathbf{a}_2) \end{cases} \tag{1}$$

and the wall–particle interaction, similarly, is characterised by the closest distance at which a particle remains in contact with the wall $\sigma_{\text{wall}}(\mathbf{a})$

$$U_{\text{wall}}(\mathbf{r}_\perp, \mathbf{a}) = \begin{cases} 0 & \text{if } |\mathbf{r}_\perp| \geqslant \sigma_{\text{wall}}(\mathbf{a}), \\ \infty & \text{if } |\mathbf{r}_\perp| < \sigma_{\text{wall}}(\mathbf{a}). \end{cases} \tag{2}$$

In above, $\mathbf{r}_{12}$ is the vector connecting the centres of two particles and $\mathbf{r}_\perp$ is the perpendicular to the wall vector that separates the particle centre from the substrate. The orientation $\mathbf{a}$ is described in terms of the polar and azimuthal angles $\mathbf{a} = (\theta, \phi)$.

Leaving a discussion on details of the shape functions σ and σ_{wall} for later we can proceed our considerations with the functional of the free energy. Its general form reads [38,39]

$$\begin{aligned} \beta\mathscr{F} = &\int \rho(\mathbf{a}, \mathbf{r})[\log \rho(\mathbf{a}, \mathbf{r}) - 1] \, \mathrm{d}\mathbf{a} \, \mathrm{d}\mathbf{r} - \frac{1}{2} \int f_{12}(1,2)\rho(1)\rho(2) \, \mathrm{d}(1) \, \mathrm{d}(2) \\ &+ \beta \int U_{\text{wall}}(z_1, \mathbf{a}_1)\rho(1) \, \mathrm{d}(1). \end{aligned} \tag{3}$$

This form is given in the second virial approximation, which takes into account only the interaction terms up to the square order in the number density (note that $\rho(\mathbf{a}, \mathbf{r})$ is proportional to the density). Such an approximation is the necessity, since only for two particles an assessment of the interaction kernel is feasible. In (3) we use the abbreviations $(1) \equiv (\mathbf{a}_1, \mathbf{r}_1)$, $\mathrm{d}(1) \equiv \mathrm{d}\mathbf{a}_1 \mathrm{d}\mathbf{r}_1$ and $f_{12} = \exp(-\beta U_{12}) - 1$ denotes the Mayer function; β stands for $1/kT$ with k denoting the Boltzmann constant and T denoting the thermodynamic temperature; $U_{\text{wall}}(z_1, \mathbf{a}_1)$ represents an external potential, in our case originating from the presence of the walls.

The functional dependence of Eq. (3) rests upon the distribution function $\rho(\mathbf{a}, \mathbf{r})$, which is defined as the probability to find a particle with the orientation $\mathbf{a}$ at the position $\mathbf{r}$ multiplied by the total number of the particles in the system in such a way that the normalisation condition holds: $\int \rho(\mathbf{a}, \mathbf{r}) \, \mathrm{d}(1) = N$. For a confined liquid crystal fluid this function is inhomogeneous with respect to the both arguments, the position and the orientation. It is not necessary to mention that these two types of inhomogeneities are, in general, coupled.

The condition for the equilibrium state is given then by the minimum of the grand canonical potential $\mathscr{F}_{\text{Grand}} = \mathscr{F} - \mu \int \rho(1) \, \mathrm{d}(1)$:

$$\frac{\delta \mathscr{F}_{\text{Grand}}}{\delta \rho} = 0, \tag{4}$$

where μ stands for the chemical potential. The condition (4) is, of course, mathematically equivalent to the conditional minimum of $\mathscr{F}$, where the imposed condition is the normalisation

$$\frac{\delta \mathscr{F}_{\mathrm{Lagr}}}{\delta \rho} = 0 \tag{5}$$

and $\mathscr{F}_{\mathrm{Lagr}} = \mathscr{F} - \mu(\int \rho(1)\,\mathrm{d}(1) - N)$. Thus, the chemical potential μ can be also interpreted as the Lagrangian multiplier.

While solving the condition (4) it is useful to introduce a new effective function which will be the factually searched for. For this purpose we chose the reference system in such a way that the Z axis is along the direction perpendicular to the walls. As long as we are interested only in nematic phases, the directions X and Y are equivalent to each other, and, since in fact our problem is one-dimensional, irrelevant.

As our working function we chose the probability

$$f(\mathbf{a}, z) = \frac{\rho(\mathbf{a}, \mathbf{r})}{L d}, \tag{6}$$

where d is the global density of the system $d = N/V$ and V is the volume. Integration concerns the whole XY cross-section areas of the liquid crystal sample. Since, due to the chosen geometry of the sample, these cross-sections are independent on z coordinate, we can use for them only one symbol, namely S^{xy}. Its value is of no importance, however its usage has helped us in manipulating the free energy functional. Normalisation of the function f given by the formula (6) agrees now with the strict condition for the probability, i.e., the integral of f over the whole available argument space equals to unity

$$\int_0^{2\pi} \int_0^{\pi} \int_0^{L} f(\theta, \varphi, z)\,\mathrm{d}z \sin\theta\,\mathrm{d}\theta\,\mathrm{d}\varphi = 1. \tag{7}$$

With the help of the formula (6) we can now substitute the function ρ with the function f in the free energy

$$\beta\mathscr{F} = \int f dL(\log f dL - 1 + \beta U_{\mathrm{wall}}(z_1, \mathbf{a}_1))\,\mathrm{d}(1) - \frac{1}{2}\int f_{12}(1,2) f_1 dL f_2 dL\,\mathrm{d}(1)\,\mathrm{d}(2). \tag{8}$$

After integration over the variables x and y one obtains

$$\begin{aligned}\beta\mathscr{F} = {} & dLS^{xy}\int f(\log f + \log Ld - 1 + \beta U_{\mathrm{wall}}(z, \mathbf{a}))\,\mathrm{d}z\,\mathrm{d}\mathbf{a} \\ & + \frac{1}{2}(dL)^2 S^{xy}\int S_{\mathrm{excl}}(\mathbf{a}_1, z_1, \mathbf{a}_2, z_2) f_1 f_2\,\mathrm{d}z_1\,\mathrm{d}\mathbf{a}_1\,\mathrm{d}z_2\,\mathrm{d}\mathbf{a}_2,\end{aligned} \tag{9}$$

where the double XY space integration of the Mayer function resulted in the area S^{xy} and a new function $S_{\mathrm{excl}}(\mathbf{a}_1, z_1, \mathbf{a}_2, z_2)$

$$\int f_{12}(1,2)\,\mathrm{d}x_1\,\mathrm{d}y_1\,\mathrm{d}x_2\,\mathrm{d}y_2 = S^{xy} S_{\mathrm{excl}}(\mathbf{a}_1, z_1, \mathbf{a}_2, z_2). \tag{10}$$

This new function is a two-dimensional counterpart of the excluded volume (henceforth called by the *excluded slice*). One can picture it as an appropriate cross-section of the excluded volume body (see Fig. 1), which should be reproduced if we add up all the slices together

$$\int S_{\mathrm{excl}}(\mathbf{a}_1, z_1, \mathbf{a}_2, z_2)\,\mathrm{d}z_1\,\mathrm{d}z_2 = L V_{\mathrm{excl}}(\mathbf{a}_1, \mathbf{a}_2). \tag{11}$$

In above V_{excl} denotes the excluded volume. The standard definition of V_{excl} represents it as the set of points in space that are not accessible by the centre of the particle, say j, whose fixed orientation is given by $\mathbf{a}_j$ in the presence of another particle, say i, also with the fixed orientation $\mathbf{a}_i$. In practice, one can imagine the excluded volume as moving the particle j all around the particle i always in contact with one another and

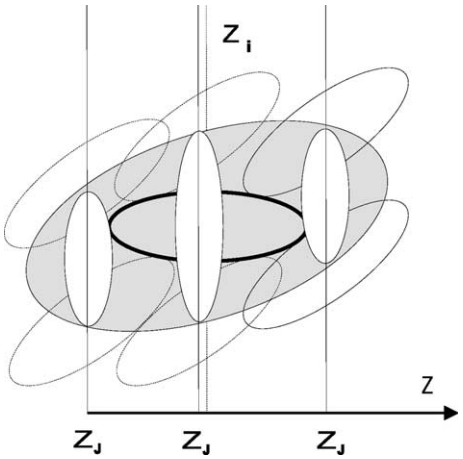

Fig. 1. An example of the excluded volume and the excluded slices. The excluded volume is obtained by moving the particle j around the particle i under the fixed orientations' condition. The subsequent positions of the particle j are drawn in a thin solid line, the particle i is drawn with a thick solid line in the middle of the picture and the excluded volume is given by the shadowed area. The excluded slices are the white ellipsoidal cross-sections and are presented for three different z_j positions of the particle j centre. Each slice is parametrised by the value of $|z_i - z_j|$.

with the fixed orientations. By analogy, one can imagine the excluded slice by moving the particle j all around the particle i but only within the plane XY, i.e., under the condition of fixed positions z_j and z_i. By the symmetry reasons S_{excl} will depend effectively on $|z_i - z_j|$. These symmetry arguments by no means hold in general. This can be seen, for example, close to the walls. The situations generated by the sets of two particles, $\{(\mathbf{a}_i, z_i), (\mathbf{a}_j, z_j)\}$ and $\{(\mathbf{a}_i, z_i'), (\mathbf{a}_j, z_j')\}$ subject to the condition $|z_i - z_j| = |z_i' - z_j'|$, are not equivalent. It is important then to realise that this fact is caused purely by the wall interactions and *not* by the nature of the *excluded slice*.

Finally one deals with the expression for the energy per particle

$$\frac{\beta\mathscr{F}}{N} = \int f(\log f + \log Ld - 1 + \beta U_{\text{wall}}(z, \mathbf{a}))\, \mathrm{d}z\, \mathrm{d}\mathbf{a} + \frac{1}{2} Ld \int S_{\text{excl}}(\mathbf{a}_1, z_1, \mathbf{a}_2, z_2) f_1 f_2\, \mathrm{d}z_1\, \mathrm{d}\mathbf{a}_1\, \mathrm{d}z_2\, \mathrm{d}\mathbf{a}_2 \tag{12}$$

and with the condition of the energy minimum $\delta\mathscr{F}/\delta f = N\mu$ that takes the following form of the self-consistency integral equations:

$$dL \int_0^L \int_0^\pi \int_0^{2\pi} S_{\text{excl}}(\mathbf{a}_1, z_1, \mathbf{a}_2, z_2) f_2(\mathbf{a}_2, z_2)\, \mathrm{d}z_2\, \mathrm{d}\mathbf{a}_2 = \mu - \log Ld - \log f(\mathbf{a}_1, z_1) - \beta U_{\text{wall}}(z_1, \mathbf{a}_1). \tag{13}$$

This is the main equation of the df theory of inhomogeneous liquid crystals considered here.

3. On solving integral equations in a polynomial expansion approach

In this section we recall the basic way of solving the self-consistency equations in a polynomial expansion approach for the spatially homogeneous liquid crystal. This is a standard and well-known technique, which is put here for the benefit of the beginners in the df theories and, also, as a reference for the inhomogeneous case. In homogeneous case the self-consistency equations are quite similar to Eq. (13)

$$\log f(\mathbf{a}_1) + d\int_0^{\pi}\int_0^{2\pi} V_{\mathrm{excl}}(\mathbf{a}_1,\mathbf{a}_2) f_2(\mathbf{a}_2)\mathrm{d}\mathbf{a}_2 = \mu - \log d. \tag{14}$$

As already suggested by the name itself, the main idea of the polynomial expansion approach is to expand the equation components, the logarithm of the distribution f and the interaction kernel V_{excl}, in terms of the symmetry adapted functions. For nematics composed of uniaxial particles these functions can be either the spherical harmonics Y_m^l or the Mulder functions Δ_{mn}^l [40], where the index n has been put to zero: $n = 0$. The uniaxial symmetry imposes that the integers l and m should be even numbers. In the case of the complex Y functions m is limited to the values $|m| \leqslant l$ and in the case of Δs to $0 \leqslant m \leqslant l$. Both descriptions, in Y and in Δ functions, should be equivalent. This entails another condition for the spherical harmonics, namely that the functions Y_m^l and Y_{-m}^l will share the same coefficient in expansions. For practical reasons the Mulder functions can be more preferred to the harmonics. Firstly, because, by definition, they are real and, secondly, because expressions for the order parameters make use of the Δ forms. As the third argument one can add the fact that the Mulder functions can be used also for the cases with molecular biaxiality. A general recipe how to obtain Δs is based on the standard Wigner functions $\mathscr{D}_{mn}^l$ [40]

$$\Delta_{m,n}^l(\Omega) = \left(\frac{1}{2}\sqrt{2}\right)^{2+\delta_{m,0}+\delta_{n,0}} \sum_{\sigma,\sigma'=\{-1,1\}} \mathscr{D}_{\sigma m,\sigma' n}^l(\Omega), \tag{15}$$

where Ω represents the Euler angles $\Omega \equiv (\theta,\phi,\psi)$. In what we present next, we give an example based on the Mulder functions. Since in the present problem the molecular biaxiality represented by the ψ dependence is not taken into account, for brevity we will skip writing the index 0: $\Delta_{m,n}^l \equiv \Delta_m^l$ and we will systematically omit the factor 2π associated to the ψ variable from the formulas. Also, instead of Ω we will use again the orientation $\mathbf{a}$, which is ascribed only to two relevant Euler angles, θ and ϕ.

The needed expansions follow:

$$V_{\mathrm{excl}} = \sum_{l,m} \frac{2l+1}{4\pi} V_{lm} \Delta_m^l(\tilde{\mathbf{a}}) \tag{16}$$

and

$$\log f(\mathbf{a}_1) = \sum_{l,m} \frac{2l+1}{4\pi} c_{lm} \Delta_m^l(\mathbf{a}_1), \tag{17}$$

where $\tilde{\mathbf{a}}$ is the relative angle between the particles with orientations $\mathbf{a}_1$ and $\mathbf{a}_2$, $\tilde{\mathbf{a}} = \mathbf{a}_1^{-1}\mathbf{a}_2$. Coefficients V_{lm} should be evaluated on the basis of the assumed interaction model before starting the iteration procedure. The unknowns to be found are the distribution coefficients c_{lm}. For a nematic, which in the most general case is biaxial, the number of independent coefficients c_{lm} is given by the biaxial symmetry rules, which say that l and $|m|$ should be even and positive numbers such that $|m| \leqslant l$.

Equations for the separate c_{lm} can be extracted from Eq. (13) by multiplying it with subsequent Δ functions and, then, by using of the orthogonality rules

$$\frac{4\pi}{2l+1}\delta_{l,l'}\delta_{m,m'} = \int \Delta_m^l(\mathbf{a})\Delta_{m'}^{l'}(\mathbf{a})\,\mathrm{d}\mathbf{a} \tag{18}$$

and the formula

$$\int V_{\mathrm{excl}}(\tilde{\mathbf{a}})\Delta_m^l(\mathbf{a}_2)\,\mathrm{d}\mathbf{a}_2 = \sum V_{l0}\Delta_m^l(\mathbf{a}_1). \tag{19}$$

In the above we have used the property

$$\int \Delta_m^l(\tilde{\mathbf{a}})\Delta_{m'}^{l'}(\mathbf{a}_2)\,\mathrm{d}\mathbf{a}_2 = \frac{4\pi}{2l+1}\delta_{l,l'}\delta_{m0}\Delta_{m'}^{l}(\mathbf{a}_1). \tag{20}$$

As a result one obtains a set of $(L_{\max}+2)(L_{\max}+4)/4$ integral equations for the coefficients c_{lm}, where $L_{\max}$ is the maximum order, which is taken into account in the excluded volume expansion (Eq. 16)

$$c_{lm} + dV_{l0}\int \Delta_m^l \exp\left[\sum_{l,m}\frac{2l+1}{4\pi}c_{lm}\Delta_m^l(\mathbf{a}_1)\right]\mathrm{d}\mathbf{a}_1 = 0. \tag{21}$$

For a given particles' number N and volume V the chemical potential μ in equilibrium is constant throughout the sample. As such, it can be obtained from

$$\mu = c_{00} + \log d + \frac{d}{4\pi}V_{00}. \tag{22}$$

In order to apply the polynomial expansion approach into the case of inhomogeneous liquid crystals let us invert Eq. (13) as

$$f(z_1,\mathbf{a}_1) = \exp\left[-d\int_0^L\int_0^\pi\int_0^{2\pi} S_{\mathrm{excl}}(z_1,\mathbf{a}_1,z_2,\mathbf{a}_2)f_2(z_2,\mathbf{a}_2)\,\mathrm{d}z_2\,\mathrm{d}\mathbf{a}_2 + \mu - \log Ld - U_{\mathrm{wall}}(z_1,\mathbf{a}_1)\right]. \tag{23}$$

It is immediately seen from Eq. (23) that for infinite wall potentials, which is the case for certain orientations corresponding to the hard core limit of the potential, the distribution function disappears. In this case, the usage of the polynomial expansion approach becomes more complicated. As the first let us discuss a simpler case of the surface potentials without any hard core. An example of such potential one can find in [41]. It reads:

$$U_{\mathrm{wall}}(z,\mathbf{a}) = \begin{cases}\epsilon(1-(\mathbf{a}\cdot\mathbf{d})^2), & |z-z_{\mathrm{wall}}| < A/2,\\ 0, & \text{otherwise},\end{cases} \tag{24}$$

where $\mathbf{a}$ is the particle orientation, $\mathbf{d}$ is the wall ordering direction and ϵ is the field strength. A denotes the length of the particle's symmetry axis. This form of the potential assumes the whole angular boundaries, i.e., (0–π) for the polar angle and (0–2π) for the azimuthal angle.

The general structure of polynomial expansions in the inhomogeneous case is not affected by the type of the wall potential and it yields

$$S_{\mathrm{excl}}(z_1,\mathbf{a}_1,z_2,\mathbf{a}_2) = \sum_{l,m} s_{lm}(z_1,z_2)\Delta_m^l(\mathbf{a}_1,\mathbf{a}_2) \tag{25}$$

and

$$\log f(z_1,\mathbf{a}_1) = \sum_{l,m} c_{lm}(z_1)\Delta_m^l(\mathbf{a}_1). \tag{26}$$

The unknowns to be solved for are now the functions $c_{lm}(z_1)$. Evaluation of them can be done only on a discrete grid and the solution of the self-consistency equations also involves the necessity to integrate over the z variable. For this purpose traditionally an equispaced grid and trapezoidal rule have been used [41]. For the surface potentials without hard cores the technique of solving the self-consistency equations is very similar as for the above discussed homogeneous case. Notice only that the chemical potential μ, which is

constant throughout the sample for a given particles' number N and volume V, now can be re-addressed as constant in respect to more suitable for the confined geometry parameters (fully equivalent to V and N): the number density d and the wall separation distance L. If the set of algebraic equations for the coefficients c_{lm} is too large and too awkward to handle, it can alternatively be used a numerical minimisation of the grand potential with respect to c_{lm}.

When the surface potential contains a hard core contribution that restricts rotations of the molecules at the walls the situation becomes much different. It can be illustrated, for instance, by the infinite potential from Eq. (2) and the closest approach $\sigma_{\text{wall}}(\mathbf{a})$ as

$$\sigma_{\text{wall}}(\mathbf{a}) \equiv z_{\text{wall}} = \frac{A}{2}\cos\theta. \tag{27}$$

The first observation now is that the orthogonality rules do not hold in the surface areas. Instead of (18) we obtain a chain of integrals which, nevertheless, knowing the restricting conditions, can be calculated. Whereas for full angular intervals the term of a given order, say $l = 2$, decouples from the terms of higher orders, in the case of restricted orientations one can deal with non-zero integrals like

$$A^{4,2}(z) = \int_{\Theta_{\max}(z)}^{\pi-\Theta_{\max}(z)} \Delta_0^4 \Delta_0^2 \sin\theta \, \mathrm{d}\theta \, \mathrm{d}\phi. \tag{28}$$

Knowing the penalty function $\Theta_{\max}(z)$ all functions of the above sort can be calculated and stored for the future usage. From the condition (27) it follows, for example, that $\Theta_{\max}(z) = \arccos(2z/A)$. Similar situation occurs in analyzing Eqs. (19) and (20).

As for the changes that occur in the way of solving the self-consistency equation (13), it follows. The expansions (25) and (26) are still valid, but extraction of the coefficients $c_{lm}(z_i)$, where z_i denotes ith point of the Z grid, gets really very complicated. For instance, new contributions appear in the integrals like

$$\int_{\Theta_{\max}(z_i)}^{\pi-\Theta_{\max}(z_i)} \log f \Delta_0^2 \sin\theta \, \mathrm{d}\theta \, \mathrm{d}\phi = A^{2,0}(z_i)c_{00}(z_i) + A^{2,2}(z_i)c_{20}(z_i) + A^{2,4}(z_i)c_{40}(z_i)\cdots, \tag{29}$$

where the numbers $A^{l,l'}$ are like in (28) which, once calculated, can be regarded as known. Although our set of algebraic equations obtains many new terms, one can still have the same number of independent equations as unknowns, hence the problem is solvable. The main difficulty is a big number of unknowns, which increases with the expansion order of the interaction kernel. This can be the reason why in practice the polynomial expansion approach (and its different implementations) for inhomogeneous media is limited to small order in Y_m^l [42] or even to the second order [41].

The method presented in next sections does not use any polynomial expansions and, moreover, includes the whole influence of the interaction kernel.

4. Gaussian integration with the adjusted angular limits

Since the problem under consideration is inhomogeneous as well in the spatial as in the orientational space, one has to take into account a description in which the functions are represented by their values on an appropriate grid. Most commonly used here is the idea of the fixed and equispaced grids [41,42]. This is imposed by the structure of the self-consistency equations and the computers efficiency, if one wants to find equations solution in an iterative manner. In most cases the interaction kernel S_{excl} from the formula (13) is

not given by any analytical form and its necessary values should be stored in matrices. On an equispaced grid it is sufficient to store and use the values only for the intervals in the relative variable $z_i - z_2$ (not for the individual points z_i). The gain is substantial. Equispaced grids, however, entail the necessity to use standard but numerically the less accurate ways to calculate integrals, that are directly based on the Riemann integral definition $\int f \, dx = \sum_x f(x) \Delta x$.

The integral to be calculated in Eq. (13) is three-dimensional. If we used an equispaced method equally in all three dimensions (without polynomial expansions) then, assuming crude grids of 50 intervals for each argument, θ, ϕ and z, we need $50 \times 50 \times 50 = 125{,}000$ evaluations of a single integrand, which, together with the normalisation conditions, makes 250,000 elements per one iteration. This requirement is certainly prohibitive for ordinary computers. What is worse, at different distances close to the wall it can be left effectively 30, 10 or 6 points for evaluations. Can one trust the assessment of an integral, which is based on a few points chosen from the equispaced set? Non-equispaced grid and the exact methods of the Gaussian quadratures offer another possibility.

At first glance, the Gaussian quadratures seem to be forgotten in the case of inhomogeneous liquid crystals. The reason for their rejection is straightforward. One cannot omit then even a single point and this is what happens, when the particles approach the wall: some of the space points that depend on the particles orientations are forbidden. It might seem, then, that we are condemned to use the equispaced grids but this impression is false.

An extensive description on this subject one can find, for example, in Numerical Recipes [37] and in references therein.

As an exact method for the multidimensional integrals Numerical Recipes [37] advises the procedure *quad3d*, which is based on sequential calling of the one-dimensional Gaussian quadrature. This procedure, *quad3d*, is written in the form that contains calls to the user-supplied integrand and the boundaries functions. Straight application of it to the confined liquid crystals is problematic for a few reasons. Firstly, not all of the integrand components can be analytically given. One of them, moreover, the distribution function, is our unknown. Also the excluded slices themselves may come from other methods like the Monte Carlo assessments. Secondly, the procedure spends substantial amount of time sweeping the areas where the integrand is zero. The third notice is that the needed order of the Gaussian quadrature for Z integrations can be much larger than for the angular integrations. *quad3d* also calculates the same abscissas for many times. These shortcomings, however, do not ban the idea itself and can be easily removed. To see that the idea of GQ works, one should only go back to the fact that the Gaussian quadratures are based, in fact, on discrete values.

In order to apply GQ to the nematic in a slab geometry let us start from the construction of all the needed Gaussian abscissas. In the z coordinate the number of the Gaussian points will be given as NGZ and the abscissas are fixed in space. The borders of integrations are given by $a = 0$ and $b = L$. Gaussian points are generated then by the standard recipe:

$$
\begin{aligned}
&xm = 0.5(b - a)\\
&xr = 0.5(b + a)\\
&for(i = 1; i <= NGZ2; i++)\\
&\{\\
&z[i] = xm - xr * x[i];\\
&z[NGZ2 + i] = xm + xr * x[i];\\
&wz[i] = w[i];\\
&wz[NGZ2 + i] = w[i];\\
&\}
\end{aligned}
\tag{30}
$$

where $NGZ2 = NGZ/2$ and $x[i]$ are the points from the interval $(0, 1)$ corresponding to the roots of the NGZ Legendre polynomial [37]. Additionally in (30) we have included the weights $wz[i]$. Note that the recipe makes use of the fact that the Gaussian points are placed symmetrically with respect to the middle point of the interval.

Integrations over the angle ϕ in Eq. (13) are independent from z and θ and can be calculated using standard Gaussian procedure of a new order of the quadrature, say, NG.

As concerns integration in θ the situation, as already discussed, gets complicated. Not all the values from the interval $(0, \pi)$ can be available. This availability depends on the distance from the wall. A construction of the Gaussian points in the polar angle in the vicinity of the substrate is presented in Fig. 2, where the wall interaction considered is just of a hard wall. One can see that the set of the Gaussian abscissas in the polar angle domain is parametrised by izth point on the axis Z. Effectively, one has the set of the θ angle points

$$
\begin{aligned}
&xmt[iz] = 0.5 * (bt[iz] + at[iz]);\\
&xrt[iz] = 0.5 * (bt[iz] - at[iz]);\\
&for(i = 1; i <= NG2; i++)\\
&\{\\
&xt[i][iz] = xmt[iz] - xrt[iz] * xt[i];\\
&xt[NG2 + i][iz] = xmt[iz] + xrt[iz] * xt[i];\\
&\}\\
&wt[i] = wwt[i];\\
&wt[MDIVT + i] = wwt[i];
\end{aligned}
\tag{31}
$$

For the limits $at[iz]$ and $bt[iz]$ the hard wall condition imposes the values

$$at[iz] = \Theta_{\max}, \tag{32}$$

$$bt[iz] = \pi - \Theta_{\max}. \tag{33}$$

Using the above information we can write now a code which gives the value of the three-dimensional integral from Eq. (13). It consists from three loops accordingly to three types of variables. Note the importance of the order of the loops, namely that the loop for the Z integration is the most outer loop!

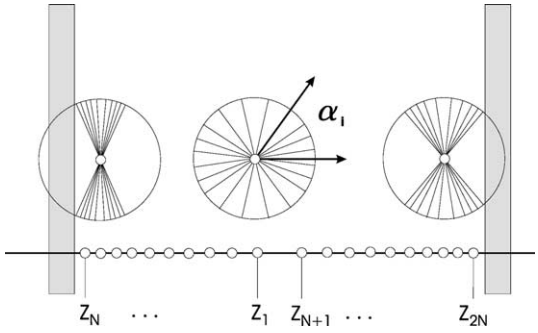

Fig. 2. Representation of the angular and the spatial Gaussian points.

```
sumaz = 0.0;
for(z2 = 1; z2 <= NGZ; z2++)
{
fz12 = fabs(z[z1] - z[z2]);
if (fz12 <= 2 * A)
{
suma = 0.0;
for(k = 1; k <= NG; k++)
{for(h = 1; h <= NG; h++)
{
help = Slice(i, j, z1, k, h, z2);
suma+ = wt[k] * wf[h] * fodf[k][h][z2] * help;
}}}
sumaz+ = wz[z2] * suma * xrf * xrt[k];
}
sumaz* = xrz;
```
(34)

In the structure of the integration procedure like in (34) it is now very easy to introduce a penalty condition to eliminate the cases where the excluded slice function is zero. The most crude condition follows the fact that the relative distance between the point belonging to the particle "1" and the point from another particle "2" $fz12 = fabs(z[z1] - z[z2])$ is larger from the longest particle cross-section. For ellipsoids the longest cross-sections coincide with the longest principal axis (in this paper denoted by the symbol A) times 2. So the inner loops in (34) are considered only if the condition $fz12 <= 2 * A$ is fulfilled.

5. Orientational and density profiles for a confined nematic

In this section we present the density functional theory results for the HGO system with respect to different integration parameters. General features of this system have already been introduced in [12] and the details on the excluded areas one can find in [43].

Our example considers the system of ellipsoidal HGO particles at the density $\rho = 0.292$. The long axis of the molecule is $A = 2.5$ and the short is given by $B = 0.5$, hence the aspect ratio equals to 5. The wall separation is four times the length of the particles. Throughout the graphic presentations we undertake the rule to present different results with respect to the fixed number of iterations, $NITER = 500$.

At the chosen density the system is in a well-ordered nematic phase. The director points towards the X axis which is established accordingly to the largest eigenvalue of the order parameter tensor $\mathbf{Q}$. A complete set of $\mathbf{Q}$ values is given in Fig. 3(a). Analysis of their behavior [12] shows the uniaxial order in the bulk area and the biaxial order at the walls. Figs. 3(b)–(d) present details of the eigenvalues Q_{xx}, Q_{yy} and Q_{zz} profiles obtained for the largest grid in Z, $NGZ = 88$, and two different NG sets used for the angular integration. There is a substantial improvement after the increase of the NG Gaussian points from 10 to 16 ranging up to the difference (absolute) of 0.015.

In Fig. 4 we present the density profiles. For the angular integration we use two sets of the Gaussian points, $NG = 10$ and $NG = 16$. More attention is paid to space integration. Here we check the results for the Gaussian sets with the number of points NGZ, 32, 44, 64, 88, respectively.

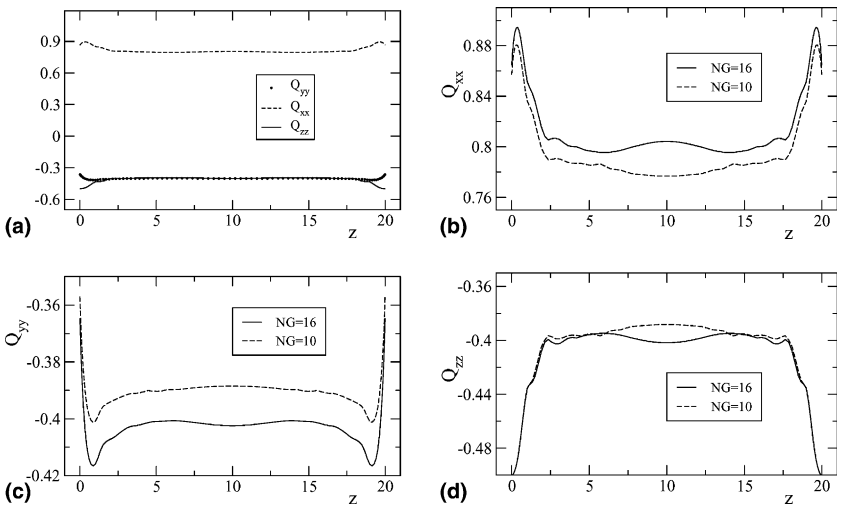

Fig. 3. (a) Three eigenvalues of the tensor **Q** calculated on a grid containing $NG = 16$ and $NGZ = 88$ points. The figures (b)–(d) present comparison between the profiles of Q_{xx}, Q_{yy} and Q_{zz} eigenvalues obtained with $NGZ = 88$ but at different number of Gaussian points in the angular integration, $NG = 10$ and $NG = 16$. To show details the scale of presentations in (b)–(d) as compared to (a) has been magnified.

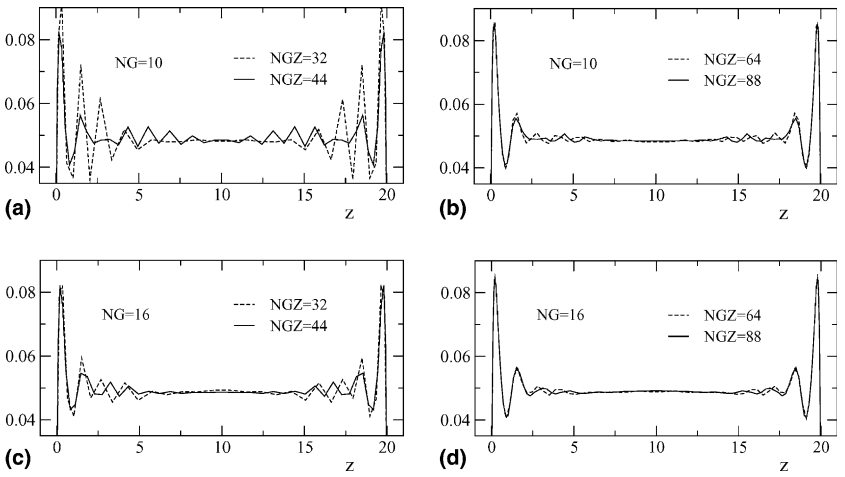

Fig. 4. The density profiles obtained after 500 iterations for different numbers of the grid points. *NG* denotes the number of the Gaussian points used in the angular integrals. (a) and (b) are for $NG = 10$ and (c) and (d) for $NG = 16$. Subsequent curves in the pictures correspond to *Z* grid of $NGZ = 32$, $NGZ = 44$, $NGZ = 64$ and $NGZ = 88$ Gaussian points. For $NGZ = 64$ and $NGZ = 88$ the density profiles are not significantly influenced by the accuracy of the angular integrals.

From Fig. 4 one sees that the number of points in the angular integration strongly influences the density profiles in the cases with small numbers of *Z* grid points. Differences in the shape of the curves in Figs. 4(a) and (c) are undeniably big. This changes for larger *Z* grids, as is shown in Figs. 4(b) and (d). Here, the structure of the surface peaks remains almost the same. An increase of the grid size, however, results with longer computational time. An optimal grid should provide a compromise between the profiles quality and the computers' fastness. Fig. 4 shows that $NGZ = 64$ gives already reasonable profiles but it is not very conclusive with respect to the angular integration.

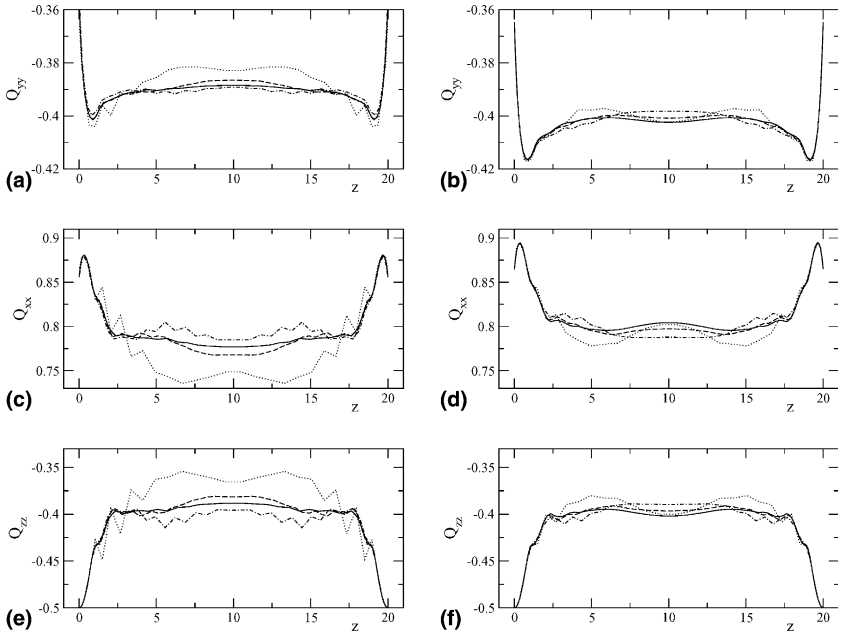

Fig. 5. Influence of the grid size on the accuracy of the order parameter profiles. (a), (c) and (e) (left column) are for the angular $NG = 10$ points and (b), (d) and (f) (right column) are for $NG = 16$. The subsequent curves in the pictures come from the usage of different Z grid density. The dotted line is for $NGZ = 32$, the dashed-dotted line for 44, the dashed line for $NGZ = 64$ and the solid line for $NGZ = 88$.

A more detailed study of the order parameters profiles presented in Fig. 5 shows again that the grid number $NG = 10$ leads to large errors for $NGZ = 32$ and $NGZ = 44$. These results indicate that inaccurate integration methods may suggest strong coupling between orientational and spatial properties which in reality is a numerical artefact. A similar effect has been encounter by Shundyak and van Roij [42], but with respect to influence of the angle responsible for biaxiality. During their investigations on isotropic–nematic interfaces and the surface biaxiality effect for the Onsager spherocylinders, the authors of [42] observed that the isotropic–nematic surface tension that follows after including biaxiality in the calculations is substantially smaller than the corresponding values based only on the uniaxial profiles in the case of the cruder grids, i.e., containing less than 200 equispaced points (this relates to an averaged number of points per particle length of 20). This difference is a numerical inaccuracy and vanishes for larger grids (more accurate spatial integration).

The error parameter we utilise is a sum of the absolute values of the differences between the old and the new iterated distribution values at each evaluated point. As such defined, the error is proportional to the number of the total Gaussian points used (the size of the grids) which in our case vary from 3200 ($10 \times 10 \times 32$) till 22,528 ($16 \times 16 \times 88$). In our calculations the convergence error varies from 0.00002 to $10E - 8$, the less accurate for the system with the smallest number of the grid points. These errors together with the large numbers of evaluations used show that the quality of the results do not couple to the convergence degree.

At the end we would like to highlight two points.

The presented analysis is for the case when the integration regimes are ''in one piece''. The integration in space spans the length $(0, L)$, the integration in the azimuthal angle $(0, 2\pi)$, and in the polar angle $(\Theta_{\max}, \pi - \Theta_{\max})$. In principle one can divide these regimes into subregimes and use for each subregime an independent integration. This is worth remembering since there are cases which may require separate integrations, for instance, when the wall interactions are prescribed on two disconnected regimes $(0, \Theta_{\max})$

and $(\pi - \Theta_{\max}, \pi)$. Different intervals in the Z coordinate can be also used with more Gaussian points in the oscillating in density regimes and less in more uniform areas. The program using independent subintervals in the integrations may react differently to the initial conditions as compared to the program based on one piece integration. Also it may exhibit different convergence ability.

6. Application of the algorithm to the soft potentials

In general the wall potentials can be continuous functions which contain strong short range repulsion as well as long range attractive parts. Accordingly to the self-consistency equations they directly contribute to the mean potentials in an additive form (23). Infinitely strong steric parts make the distribution function $f(\mathbf{r}_{12}, \mathbf{a}_1, \mathbf{a}_2)$ vanish. This fact, on the other hand, influences values of all the integrals that contain f. The condition for vanishing f means that certain regimes of the integral arguments are forbidden. These regimes can be analytically assessed, for instance, with the help of the the equipotential surfaces

$$U(\mathbf{r}_\perp, \mathbf{a}_1) = 0. \tag{35}$$

A particular example of Eq. (35) of the Lennard–Jones type potential one can find in [34], where Gruhn et al. treat the walls as built from spherical particles. For a given orientation $\mathbf{a}_1$ of a chosen molecule, Eq. (35) provides the distance to the wall $|\mathbf{r}_\perp|$ below which the potential exhibits a steep slope that quickly approaches infinity. If needed the point $|\mathbf{r}_\perp|$ can be also shifted to lower values by ascribing a positive number C to the right-hand side of (35) such as $\exp(-C)$ establishes accuracy with which we need to calculate our distribution function f.

7. On the possible problems while using Gaussian integrations

The main idea of the method discussed in this paper is to preserve the number of points used for the integration in the angular intervals, especially in the subsurface areas. These angular integrations are performed by use of the Gaussian quadratures since the dependencies here, together with their derivatives, are expected to be continuous functions. Also the spatial integration over the Z variable is based here on the Gaussian quadratures. One can, however, pose the question what will happen when the interactions have discontinuous derivatives in the spatial variable, which can be encountered, for instance, in the hard particles models. In the case of such interactions one can expect that the profiles can contain cusp-like structures due to the characteristic points as, for instance, the point $Z = A/2$. Here, indeed, discontinuities of the first derivative of the obtained profiles are observed for dilute systems [12]. If the density increases, however, these cusp-like structures are getting suppressed. In view of the above one can pose the question how the Gaussian quadratures cope with such discontinuities. It is well known that high performance of the Gaussian integrations is restricted to continuous functions. In the case of cusp-like structure its efficiency deteriorates and, effectively, accuracy can reach the level of other methods as, for instance, the method based on the trapezoid rule. Still it seems that Gaussian quadratures can perform better. Let us compare accuracies for both the methods, Gaussian and trapezoid, at different numbers of the integration points.

Table 1
Accuracy of the integral of the function $y = x^2$ over the interval $[0, 1]$ in percentages ($100\% \times$ error/value)

10 Gaussian points	$10^{-13}\%$
100 Points in trapezoid method	$10^{-2}\%$
1000 Points in trapezoid method	$10^{-4}\%$
10,000 Points in trapezoid method	$10^{-6}\%$

Table 2
Accuracy of the integral of the function $y = |x|$ over the interval $[-1, 1]$ in percentages (100% × error/value)

10 Gaussian points	0.75%
20 Gaussian points	0.2%
88 Gaussian points	0.01%
101 Points in trapezoid method	0.01%
1001 Points in trapezoid method	10^{-4}%
10,001 Points in trapezoid method	10^{-6}%

In Tables 1 and 2 we give accuracies of the integrations of the cusp function $y = |x|$ and the continuous function $y = x^2$. The accuracy of the Gaussian quadrature has diminished drastically if the cusp occurred, but the trapezoid method is not much better. In practice, the accuracy of the trapezoid method can lead to much worse results since usually the functional dependencies are not linear as in the case of the parts of the function $y = |x|$, for which the trapezoid method gives perfect results.

To sum up: although the Gaussian quadratures method of integration is regarded as exact one should be aware of the fact that occurrence of the cusps in the characteristics of the confined hard core liquid crystals can influence the overall accuracy of the df theory calculations.

8. Summary

To summarise, we describe an algorithm for quick and efficient calculations of multidimensional integrals in the density functional theory of the confined liquid crystals, where the restricting conditions are imposed on the angular argument by the surface excluded volume effects that arise due to the hard core parts of the potentials. The algorithm is based on the Gaussian quadratures, whose points are parametrised by the appropriate wall conditions. In the case described it concerns integration over the polar angle and the parameter is provided by the Z dependence. Application is discussed within the framework of the simple Onsager theory, note, however, that more advanced mean field models like the Parsons–Lee theory [44] or the modified Rosenfeld theory [45] utilise similar multidimensional integrals. The algorithm uses minimal storage of the computer memory and at the same time it is capable to obtain the full information about the density oscillations and orientational (biaxial included) effects, which are characteristical for liquid crystals confined in a pore.

It has very good perspectives for future applications to more complicated problems of mixtures, smectic phases and structured substrates with a designed geometry of interactions.

References

[1] C. Ebner, W.F. Saam, New phase-transition phenomena in thin argon films, Phys. Rev. Lett. 38 (1977) 1486.
[2] W.F. Saam, C. Ebner, Classical fluid structure near solid substrates: a comparison of different theories, Phys. Rev. A 17 (1978) 1768.
[3] T.F. Meister, D.M. Kroll, Density-functional theory for inhomogeneous fluids: application to wetting, Phys. Rev. A 31 (1985) 4055.
[4] J.E. Finn, P.A. Monson, Pre-wetting at a fluid–solid interface via Monte Carlo simulation, Phys. Rev. A 39 (1989) 6402.
[5] P.I. Ravikovitch, A. Vishnyakov, A.V. Neimark, Density functional theories and molecular simulations of adsorption and phase transitions in nanopores, Phys. Rev. E 64 (2001), 011602-1, and reference therein.
[6] H. Dominguez, M.P. Allen, R. Evans, Monte Carlo studies of the freezing and condensation transitions of confined fluids, Mol. Phys. 96 (1999) 209, and reference therein.
[7] R. Evans, Fluids adsorbed in narrow pores: phase equilibria and structure, J. Phys.: Condens. Matter 2 (1990) 8989.
[8] R. Evans, in: D. Henderson (Ed.), Fundamentals of Inhomogeneous Fluids, Dekker, New York, 1992.

[9] A. Poniewierski, R. Holyst, Nematic alignment at a solid substrate: the model of hard spherocylinders near a hard wall, Phys. Rev. A 38 (1988) 3721.
[10] A. Poniewierski, Ordering of hard needles at a hard wall, Phys. Rev. E 47 (1993) 3396.
[11] Y. Mao, P. Bladon, H.N.W. Lekkerkerker, M.E. Cates, Density profiles and thermodynamics of rod-like particles between parallel walls, Mol. Phys. 92 (1997) 151.
[12] A. Chrzanowska, P.I.C. Teixeira, H. Ehrentraut, D.J. Cleaver, Ordering of hard particles between hard walls, J. Phys.: Condens. Matter 13 (2001) 4715.
[13] Z.Y. Chen, S.M. Cui, Orientational wetting layer of semiflexible polymers near a hard wall, Phys. Rev. E 52 (1995) 3876.
[14] R. van Roij, M. Dijkstra, R. Evans, Orientational wetting and capillary nematization of hard-rod fluids, Europhys. Lett. 49 (2000) 350.
[15] R. van Roij, M. Dijkstra, R. Evans, Interfaces, wetting and capillary nematization of a hard-rod fluid: theory for the Zwanzig model, J. Chem. Phys. 113 (2000) 7685.
[16] M. Dijkstra, R. van Roij, R. Evans, Wetting and capillary nematization of a hard-rod fluid: a simulation study, Phys. Rev. E 63 (2001), 051703-1.
[17] A.J. McDonald, M.P. Allen, F. Schmid, Surface tension of the isotropic–nematic interface, Phys. Rev. E 63 (2001) 010701(R).
[18] I. Rodriguez-Ponce, J.M. Romero-Enrique, L.F. Rull, Orientational transitions in a nematic liquid crystal confined by competing surfaces, Phys. Rev. E 64 (2001), 51704-1.
[19] G. Skacej, A.L. Alexe-Ionescu, G. Barbero, S. Zumer, Surface-induced nematic order variations: intrinsic anchoring and subsurface director deformations, Phys. Rev. E 57 (1998) 1780.
[20] T.Z. Qian, P. Sheng, Liquid-crystals phase transitions induced by micro-textured substrates, Phys. Rev. Lett. 77 (1996) 4564.
[21] T.Z. Qian, P. Sheng, Orientational states and phase transitions induced by micro-textured substrates, Phys. Rev. E 55 (1997) 7111.
[22] F.C. Frank, On the theory of liquid crystals, Discuss. Faraday Soc. 25 (1958) 19.
[23] M.P. Allen, Molecular simulation and theory of liquid crystal surface anchoring, Mol. Phys. 96 (1999) 1391.
[24] D.J. Cleaver, P.I.C. Teixeira, Discontinuous structural transition in a thin hybrid liquid crystal film, Chem. Phys. Lett. 338 (2001) 1.
[25] L. Harnau, S. Dietrich, Fluids of platelike particles near a hard wall, Phys. Rev. E 65 (2002) 021505.
[26] M.K. Challam, K.E. Gubbins, E. De Miguel, L.F. Rull, A molecular simulation of a liquid crystal model: bulk and confined fluid, Mol. Sim. 7 (1991) 357.
[27] G.D. Wall, D. Cleaver, Computer simulation studies of confined liquid-crystal system, Phys. Rev. E 56 (1997) 4306.
[28] J. Stelzer, P. Galatoa, G. Barbero, L. Longa, Molecular dynamics simulations of surface-induced ordering in a nematic liquid crystal, Phys. Rev. E 55 (1997) 477.
[29] Z. Pawlowska, T.J. Sluckin, G.F. Kventsel, Systematics of wetting and layering phenomena in smectic materials, Phys. Rev. A 38 (1988) 5342.
[30] J.V. Selinger, D.R. Nelson, Density-functional theory of nematic and smectic-A order near surfaces, Phys. Rev. A 37 (1988) 1736.
[31] L. Mederos, D.E. Sullivan, Smectic-A ordering at a liquid–vapor interface, Phys. Rev. A 46 (1992) 7700.
[32] Z. Zhang, A. Chakrabarti, O.G. Mouritsen, M.J. Zuckermann, Substrate-induced bulk alignment of liquid crystals, Phys. Rev. E 53 (1996) 2461.
[33] V. Palermo, F. Biscarini, C. Zannoni, Abrupt orientational changes for liquid crystals adsorbed on a graphite surface, Phys. Rev. E 57 (1998) R2519.
[34] T. Gruhn, M. Schoen, Substrate-induced order in confined nematic liquid-crystal film, J. Chem. Phys. 108 (1998) 9124.
[35] P.I.C Teixeira, A. Chrzanowska, G.D. Wall, D.J. Cleaver, Density functional theory of a Gay–Berne film between aligning walls, Mol. Phys. 99 (2001) 889.
[36] A.M. Somoza, L. Mederos, D.E. Sullivan, Wetting and layering transition in liquid crystals, Phys. Rev. E 52 (1995) 5017.
[37] W.H. Press, S.A. Teukolsky, W.T. Vetterling, B.P. Flannery, Numerical Recipes in C : The Art of Scientific Computing, second ed., Cambridge University Press, Cambridge, 1993.
[38] L. Onsager, The effects of shape on the interaction of colloidal particles, Ann. N. Y. Acad. Sci. 51 (1949) 627.
[39] For a review see e.g. G.J. Vroege, H.N.W. Lekkerkerker, Phase transitions in lyotropic colloidal and polymer liquid crystals, Rep. Prog. Phys. 55 (1992) 1241.
[40] B. Mulder, Isotropic-symmetry breaking bifurcations in a class of liquid crystal models, Phys. Rev. A 39 (1989) 360.
[41] M.P. Allen, Molecular simulation and theory of the isotropic–nematic interface, J. Chem. Phys. 112 (2000) 5447.
[42] K. Shundyak, R. van Roij, Isotropic–nematic interfaces of hard-rod fluids, J. Phys.: Condens. Matter 13 (2001) 4789.
[43] E. Velasco, L. Mederos, A theory for the liquid-crystalline phase behavior of the Gay–Berne model, J. Chem. Phys. 109 (1998) 2361.
[44] J.D. Parsons, Nematic ordering in a system of rods, Phys. Rev. A 19 (1979) 1225;
S.-D. Lee, A numerical investigation of nematic ordering based on a simple hard-rod model, J. Chem. Phys. 87 (1987) 4972;
S.-D. Lee, The Onsager-type theory for nematic ordering of finite-length hard ellipsoids, J. Chem. Phys. 89 (1988) 7036.
[45] G. Cinacchi, F. Schmid, Density functional for anisotropic fluids, J. Phys.: Condens. Matter 14 (2002) 12223.